Cell Reports
Physical Science

CellPress
OPEN ACCESS

Article

Reversible molecular motional switch based on circular photoactive protein oligomers exhibits unexpected photo-induced contraction

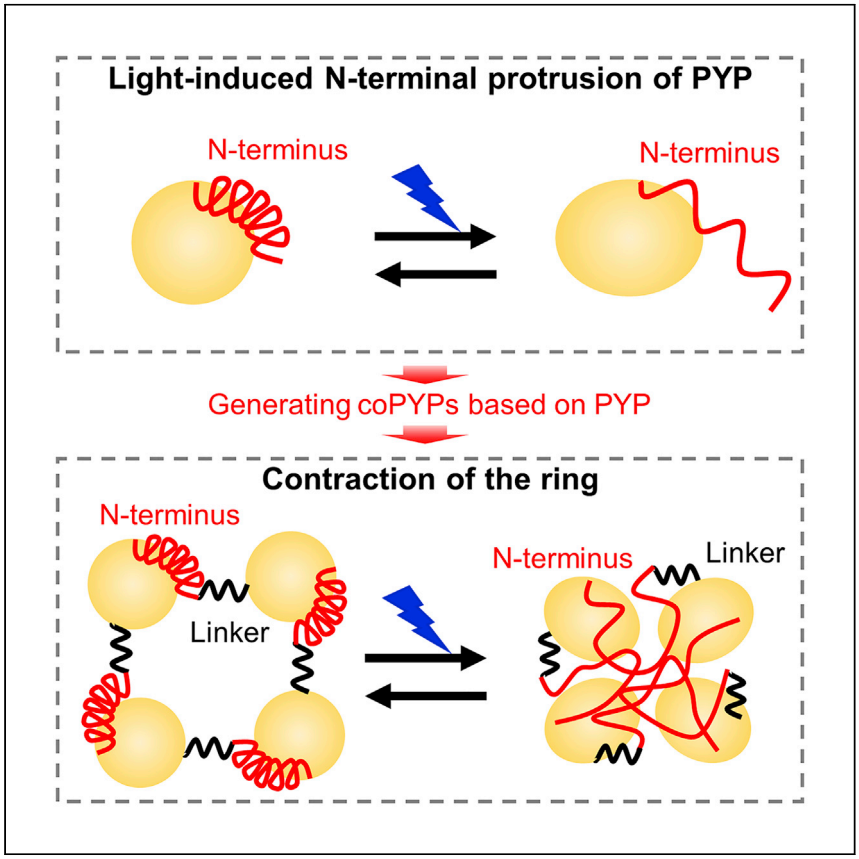

Lee et al. report molecular switches, ring-shaped circular oligomer PYPs (coPYPs), designed and generated to exploit the structural and photochromic properties of photoactive yellow protein (PYP). X-ray scattering and structural analysis of coPYP-4 show that the photoproduct of coPYPs undergoes contraction of the ring.

Sang Jin Lee, Youngmin Kim, Tae Wu Kim, ..., Hyeongseop Jeong, Jaekyung Hyun, Hyotcherl Ihee

hyotcherl.ihee@kaist.ac.kr

Highlights

Photoactive yellow protein (PYP) exhibits N-terminal protrusion by blue light

Circular oligomer PYPs (coPYPs) are designed based on PYP

It is expected that light-activated coPYPs will exhibit ring expansion

Contrary to the expectation, coPYPs undergo ring contraction

Lee et al., Cell Reports Physical Science 2, 100512
August 18, 2021
https://doi.org/10.1016/j.xcrp.2021.100512

Cell Reports
Physical Science

CellPress
OPEN ACCESS

Article

Reversible molecular motional switch based on circular photoactive protein oligomers exhibits unexpected photo-induced contraction

Sang Jin Lee,[1,2,5] Youngmin Kim,[1,2,5] Tae Wu Kim,[1,2] Cheolhee Yang,[1,2] Kamatchi Thamilselvan,[1,2] Hyeongseop Jeong,[3] Jaekyung Hyun,[3,4] and Hyotcherl Ihee[1,2,6,*]

SUMMARY

Molecular switches alterable between two stable states by environmental stimuli, such as light and temperature, offer the potential for controlling biological functions. Here, we report a circular photoswitchable protein complex made of multiple protein molecules that can rapidly and reversibly switch with significant conformational changes. The structural and photochromic properties of photoactive yellow protein (PYP) are harnessed to construct circular oligomer PYPs (coPYPs) of desired sizes. Considering the light-induced N-terminal protrusion of monomer PYP, we expected coPYPs would expand upon irradiation, but time-resolved X-ray scattering data reveal that the late intermediate has a pronounced light-induced contraction motion. This work not only provides an approach to engineering a novel protein-based molecular switch based on circular oligomers of well-known protein units but also demonstrates the importance of characterizing the structural dynamics of designed molecular switches.

INTRODUCTION

Molecular switches are molecules that can reversibly switch between two stable states in response to external stimuli such as light, temperature, voltage, pH, and ligands.[1–11] These mechanical movements of the molecular switches are closely related to biological processes such as cell metabolism, gene regulations, and allosteric regulations of enzymes.[12–17] Therefore, engineering molecular switches is of great interest not only in understanding biological processes but also in constructing artificial molecular switches with unique structural and functional properties. Particularly in recent years, protein-based molecular switches have attracted considerable attention as basic building blocks of synthetic biology because of the potential of proteins to control various biological functions.[18]

For protein-based molecular switches to perform specific functions, the structural changes of the molecular switches to the external environment must be precisely controlled. To this end, the molecular switches need to be composed of protein-building blocks with well-organized structural changes to specific stimuli. In addition, applying such molecular switches to the regulation of biological processes requires a thorough understanding of their structural mechanisms. For the functionalization of the molecular switches, various approaches have been developed based on the structural and functional properties of proteins,[19–24] as well as protein-protein,[25,26] protein-DNA,[27,28] and protein-RNA[28–30] interactions. These approaches have successfully engineered monomeric proteins to function as molecular

[1]Department of Chemistry and KI for the BioCentury, Korea Advanced Institute of Science and Technology (KAIST), Daejeon 34141, Republic of Korea

[2]Center for Nanomaterials and Chemical Reactions, Institute for Basic Science (IBS), Daejeon 34141, Republic of Korea

[3]Center for Research Equipment, Korea Basic Science Institute (KBSI), Cheongju-si, Chungcheongbuk-do 28119, Republic of Korea

[4]Molecular Cryo-Electron Microscopy Unit, Okinawa Institute of Science and Technology (OIST), Okinawa 904-0495, Japan

[5]These authors contributed equally

[6]Lead contact

*Correspondence: hyotcherl.ihee@kaist.ac.kr

https://doi.org/10.1016/j.xcrp.2021.100512

Please cite this article in press as: Lee et al., Reversible molecular motional switch based on circular photoactive protein oligomers exhibits unexpected photo-induced contraction, Cell Reports Physical Science (2021), https://doi.org/10.1016/j.xcrp.2021.100512

switches. However, except for a fold-switchable protein complex,[25] molecular switches based on complex or assembly have rarely been reported. Moreover, due to the structural complexity of proteins, the structural changes of the molecular switches to specific stimuli have not been fully characterized in most studies.

To overcome the challenges, here, we constructed a novel photoswitchable protein complex in which the structural transition is controlled by light and characterized the light-induced structural dynamics of the photoswitchable protein complex with a time-resolved structural tool. For the structural stability of the protein complex, we aimed to apply a circular shape to the complex, considering that circular proteins have higher stability against thermal, chemical, and enzymatic denaturation than do linear proteins.[31] To this end, we extended and applied the approach to constructing circularly permuted protein[21] in our study. To implement photoswitchable properties, the complex was engineered based on the structural and photochromic properties of photoactive yellow protein (PYP).[32–47]

We noticed that the photochromic properties of PYP, with its conformational change in the presence of light, give it the potential to be an excellent building block for this purpose. PYP is small (14 kDa), stable, easily expressed, and highly soluble.[48] Furthermore, PYP has a dark compact state, pG, and a light-activated state, pB_2, which has a protruding N terminus.[32,33,36,37] Because the pG state switches to the pB_2 state with blue-light irradiation in a reversible manner, PYP can be an effective protein switch. The merits of PYP for the development of molecular switches include its reversible property, allowing numerous reaction cycles; the easy detection of the dark- and light-activated states; a high quantum yield in photoconversion; and retention of the properties of PYP in molecular switches.

Using the properties of PYP, we construct circular oligomer PYPs (coPYPs), which are photoswitchable protein complexes produced in various sizes depending on the number of monomer PYP units, e.g., trimer, tetramer, and pentamer, enabling the production of coPYPs of various sizes. After the construction, we use transmission electron microscopy (TEM), transient absorption (TA) spectroscopy,[44,49,50] static X-ray solution scattering,[51–54] and time-resolved X-ray solution scattering (TRXSS), also known as time-resolved X-ray liquidography (TRXL),[33,36,55–80] on coPYP-4, a coPYP consisting of four monomer PYP units, to characterize structural and photoswitchable properties of coPYPs. TEM images show that the shape of coPYP-4 was controlled as we intended, and kinetic analysis of the TA profiles confirms that the photochromic property of monomer PYP is maintained even in the monomer PYP units composing coPYP-4. Furthermore, we identify the light-induced structural transitions of coPYP-4 involving contraction motion from the ground state to the light-activated state via the structural analysis of time-resolved and static X-ray scattering profiles from coPYP-4 based on the ensemble optimization method (EOM).[60,81,82]

RESULTS AND DISCUSSION

Design of circular tetramer PYP

Based on the light-induced N-terminal protrusion of PYP (Figure 1A),[33,35,36,38,39] we constructed coPYPs to generate photoactive oligomeric protein. For example, in the design of coPYP-4, the N terminus of each monomer PYP unit is connected to the C terminus of another monomer PYP unit by a linker (Figure 1), with the expectation that the light-induced N-terminal protrusion would move the PYP units away from one another and cause coPYP-4 to expand (Figure 1B).

Please cite this article in press as: Lee et al., Reversible molecular motional switch based on circular photoactive protein oligomers exhibits unexpected photo-induced contraction, Cell Reports Physical Science (2021), https://doi.org/10.1016/j.xcrp.2021.100512

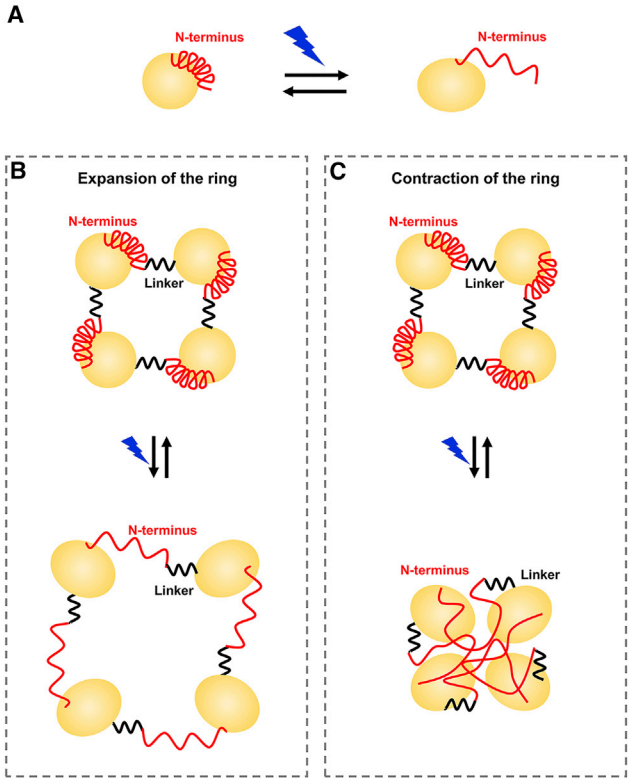

Figure 1. Schematics for the structural changes of a circular PYP oligomer controlled by light
(A) Light-induced N-terminal protrusion of monomer PYP.
(B) Expected structural change of coPYP-4: expansion of the ring.
(C) Observed structural change of coPYP-4: contraction of the ring.
The N terminus and the rest of the protein body are represented by red lines and yellow spheres, respectively. The blue lightning symbols represent light.

For the construction of coPYP-4, we first generated circularly permuted PYP (cPYP), a modified PYP connecting the N terminus and the C terminus of the target protein[21] (Figure S2A). Subsequently, we made linear trimer PYP (loPYP-3) in which three monomer PYP units are linearly connected by two flexible GS (glycine-serine) linkers (GGSGGSGG), as depicted in Figure S2B. Finally, cPYP and loPYP-3 were genetically linked by two linkers to generate coPYP-4 (Figure S2C). Here, flexible linkers were used, rather than rigid linkers, to prevent steric hindrance between the N termini in the PYP units and the linkers. We extended our approach to generating various variants of coPYP, such as circular trimer PYP (coPYP-3) and circular pentamer PYP (coPYP-5). For the construction of coPYP-3 and coPYP-5, we generated dimer PYP (PYP2) and linear tetramer PYP (loPYP-4), and each protein was genetically linked to cPYP by the two linkers as in coPYP-4 (Figures S2B and S2C). Details on the construction and preparation of the proteins are described in Supplemental experimental procedures and Figures S1 and S2.

Oligomer state of coPYPs

After construction, coPYPs were overexpressed in *Escherichia coli* BL21 (DE3) and purified by Ni affinity chromatography and ion-exchange chromatography. Monomer PYP, PYP2, and loPYP-4 were also overexpressed and purified for comparison with coPYPs. For the purified proteins, we first measured the molecular weights of

Please cite this article in press as: Lee et al., Reversible molecular motional switch based on circular photoactive protein oligomers exhibits unexpected photo-induced contraction, Cell Reports Physical Science (2021), https://doi.org/10.1016/j.xcrp.2021.100512

Table 1. The molecular weights and sizes of monomer PYP (PYP), dimer PYP (PYP2), trimer circular PYP (coPYP-3), tetramer circular PYP (coPYP-4), and pentamer circular PYP (coPYP-5) were measured by MALDI-TOF, MALS, and DLS

	PYP	PYP2	coPYP-3	coPYP-4	coPYP-5
MALDI-TOF	14 kDa	28.3 kDa	44.8 kDa	59.0 kDa	73.9 kDa
MALS	ND[a]	29.8 kDa	47.9 kDa	55.9 kDa	ND
DLS	3.8 nm	4.8 nm	7.0 nm	8.2 nm	9.2 nm

[a]ND, not determined.

monomer PYP, PYP2, and coPYPs using matrix-assisted laser desorption/ionization time-of-flight (MALDI-TOF) and multi-angle light scattering (MALS). From MALDI-TOF, the molecular weight of each protein from monomer PYP to PYP2, coPYP-3, coPYP-4, and coPYP-5 was measured as 14.0, 28.3, 44.8, 59.0, and 73.9 kDa, respectively, and MALS showed similar values for the molecular weights (Table 1). Considering the molecular weight of monomer PYP, which was ~14 kDa, the result indicates that PYP2, coPYP-3, coPYP-4, and coPYP-5 consist of two, three, four, and five monomer PYP units, respectively, as we intended. The successful construction of coPYPs is supported by native-PAGE analysis, which shows that the bands of the proteins are separated at regular intervals (Figure 2A). We also measured the size of each protein using dynamic light scattering (DLS), and the measured sizes show a tendency to increase as the number of monomer PYP units increases, as in the case of the molecular weights (Table 1).

We also used size-exclusion chromatography (SEC) on the proteins. The elution profiles of the proteins show that the elution volume decreases as the number of the PYP units increases. This result is consistent with the changes in the molecular weights of the proteins (Figure 2B). We also measured the elution profile of loPYP-4 for comparison with that of coPYP-4. Comparing the elution profiles for the two proteins shows that the elution volume of coPYP-4 is smaller than that of loPYP-4 (Figure 2B).

In addition, we collected TEM images of coPYP-4 to obtain direct information on the shape of the protein. As shown in Figure 2C, the TEM images show that the shape of coPYP-4 is circular. In particular, the images confirm that coPYP-4 is a ring-shaped protein with a central cavity, which is consistent with our design (Figure 1). Unfortunately, the small molecular weight (~60 kDa) and the flexibility of the linkers connecting the PYP units did not allow the reconstruction of the 3D structure for coPYP-4 using TEM.

Transient absorption spectroscopy

To determine the chromophore kinetics of coPYP-4, TA[49,50,83,84] signals at three wavelengths were measured and fitted simultaneously by using sums of four exponentials. As a result, we obtained four time constants of 1.9 $\pm$ 1.6 μs, 180 $\pm$ 60 μs, 1.4 $\pm$ 0.3 ms, and 79 $\pm$ 3 ms for coPYP-4 and 6.2 $\pm$ 6.4 μs, 280 $\pm$ 110 μs, 1.3 $\pm$ 0.6 ms, and 110 $\pm$ 3 ms for monomer PYP (Supplemental experimental procedures; Figure S3). The last time constant of coPYP-4 (79 ms) is slightly smaller than that of monomer PYP (110 ms), whereas the other time constants of coPYP-4 are the same as those of monomer PYP within the error ranges. To track spectral changes during the photoreaction of PYP, we measured TA spectra of coPYP-4 and monomer PYP at time delays of 100 ns, 1 μs, 10 μs, 100 μs, 1 ms, and 10 ms (Figure S3A). The different TA spectra of coPYP-4 show more negative differences than those of monomer PYP, especially in the long-wavelength region (~480 nm). The different shapes

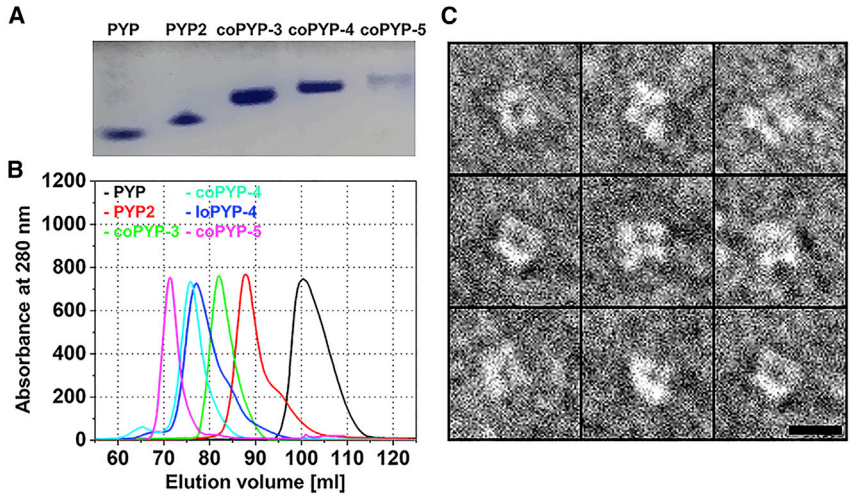

Figure 2. Native-PAGE analysis, size-exclusion chromatography, and transmission electron microscopy images of the PYP oligomers

(A) Native-PAGE analysis of the PYP oligomers. From left to right, lanes correspond to the size marker, monomer PYP (PYP), dimer PYP (PYP2), trimer circular PYP (coPYP-3), tetramer circular PYP (coPYP-4), and pentamer circular PYP (coPYP-5).

(B) Elution profiles of monomer PYP and PYP oligomers obtained from size-exclusion chromatography (SEC). The elution profile of linear tetramer PYP (loPYP-4) is also shown in this figure and compared with that of coPYP-4.

(C) Raw transmission electron microscopy (TEM) images of coPYP-4. The size of coPYP-4 is ~10 nm or less. The scale bar represents 10 nm.

of TA spectra and the faster kinetics of coPYP-4 compared with monomer PYP suggest that the local protein structure adjacent to the chromophore of each PYP unit of coPYP-4 is affected by the presence of the other units.

Time-resolved X-ray solution scattering

To investigate the light-induced structural changes of coPYP-4, we measured TRXSS data from 3.16 μs to 178 ms. As described in the Supplemental experimental procedures, the TRXSS measurements were implemented in the photosaturated regime (see Experimental Procedures for experimental details of TRXSS). Therefore, we presumed that upon the irradiation of a laser pulse, the monomeric units in coPYP-4 can be simultaneously photoexcited. The difference scattering curves, $\Delta S(q, t)$, depicted in Figure 3A show a decrease of scattering intensity in the small-angle region ($q < 0.2$ Å^{-1}) on the microsecond timescale. As the reaction proceeds in the millisecond timescale, the formation of a significant negative peak was observed in the small-angle region. However, in the wide-angle region (0.3 Å^{-1} < q < 1.0 Å^{-1}), the difference curves show only marginal features over the entire timescale. In the TRXSS data, the standard deviation is significantly smaller than the amplitude of signal intensity at each q point (Figure S4). Such low standard deviations indicate the high repeatability and reproducibility of the repeated measurements, implying that the reversibility of coPYP-4 was maintained more than 150 cycles (see Supplemental experimental procedures for the reversibility of coPYP-4). The scattering signal of the solvent heating induced by the pump laser, which contributes to the TRXSS signals in the wide-angle region, was removed using a well-established protocol[59,60] (Supplemental experimental procedures; Figure S5). To obtain the details of kinetics for these light-induced behaviors, we performed the global kinetic analysis on the heat-free difference scattering curves, $\Delta S(q, t)$, in the q range between 0.04643 and 0.9981 Å^{-1}. The global

Please cite this article in press as: Lee et al., Reversible molecular motional switch based on circular photoactive protein oligomers exhibits unexpected photo-induced contraction, Cell Reports Physical Science (2021), https://doi.org/10.1016/j.xcrp.2021.100512

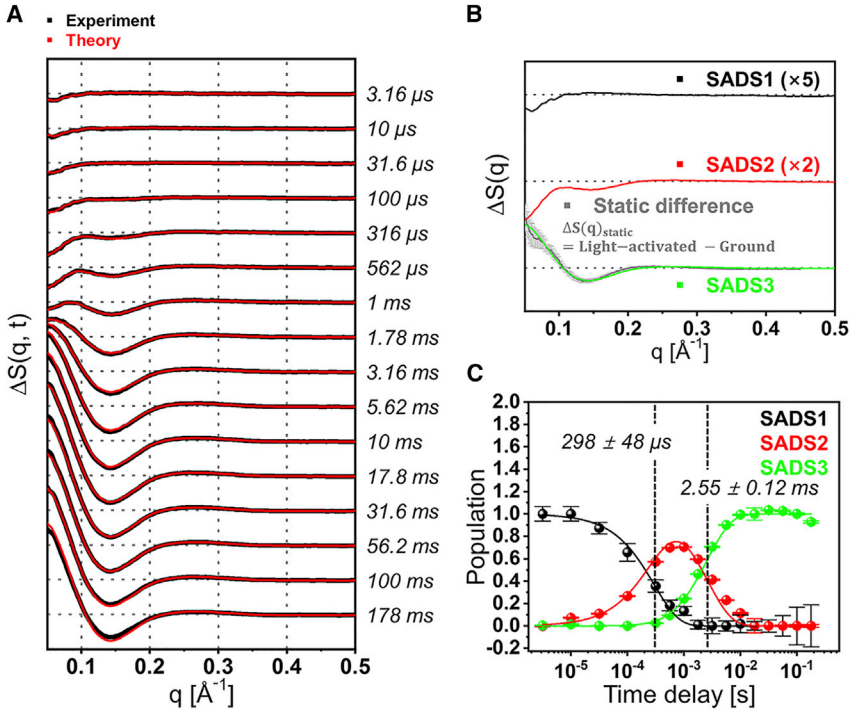

Figure 3. TRXSS data for coPYP-4 and results of kinetic analysis

(A) Experimental (black) and theoretical (red) difference scattering curves.

(B) SADSs extracted by applying SVD and PCA. SADS3 (green) compared with the static difference curve (light-activated state − ground state) from static X-ray scattering data (gray). The comparison shows high similarity between SADS3 and the static difference curve, which confirms the consistency between the TRXSS and the static X-ray scattering experiments conducted for the same light-induced transition. The error bar in the static difference is the experimental standard deviation for the static data.

(C) Time-dependent population changes of the species. The time constants are also shown. The experimental population changes (dots) are in good agreement with the theoretical population changes (lines) within the experimental errors (bars).

kinetic analysis was achieved by applying singular value decomposition (SVD) and principal-component analysis (PCA), and the details of the analysis are described in Supplemental experimental procedures.

From the SVD analysis, we identified three structurally distinct kinetic species and two time constants of 298 (±48) μs and 2.55 (±0.12) ms (Figure S6). Using these results, we applied a sequential kinetic model for the light-induced transitions involving three kinetic species and two time constants to the subsequent PCA and obtained time-independent species-associated difference scattering curves (SADSs) containing direct information on the structures of the kinetic species (Figure 3B). In this kinetic model, the formation of the first species occurs before the microsecond timescale. Subsequently, the second species is formed from the first species with a time constant of 298 μs and converts into the third species with a time constant of 2.55 ms. The theoretical difference curves reconstructed by linear combinations of the three SADSs show good agreement with the experimental curves, confirming that the sequential kinetic model is suitable for describing the experimental data (Figure 3A). The first SADS (SADS1) and the second SADS (SADS2) have a relatively small and negative intensity in the small-angle region, whereas the third SADS (SADS3) shows a prominent negative peak with a significant amplitude around

0.15 $Å^{-1}$. The difference signals of SADSs appear mostly in the small-angle range ($q < 0.2$ $Å^{-1}$), implying that coPYP-4 is subject to structural changes that affect the global shape of the protein. The difference in scattering intensity of SADSs indicates that the transition from the first species to the third species involves sequential structural changes leading from relatively small changes to large changes. The time-dependent populations of SADSs, which reflect the population changes of the relevant species, are shown in Figure 3C.

Structural analysis using the combination of the EOM analysis and MD simulations

The NMR study reported an ensemble of 26 structures for monomer PYP in the pG state,[85] and these structures showed that the N terminus of the protein is structurally flexible in the solution phase. This study suggests that the flexibility of the N terminus of each monomer PYP unit constituting coPYP-4 is likely to make the structure of coPYP-4 flexible in the solution phase. Therefore, we considered it risky to apply a single conformation to the structural analysis of coPYP-4 as in the structural analysis of well-structured proteins. Recently, a study on protein folding dynamics showed that a combination of EOM analysis and molecular dynamics (MD) simulations could describe the structural dynamics of the proteins in the flexible systems.[60] To overcome the limitation of adopting a single conformation, we employed the same approach to the structural analysis of coPYP-4.

Before this structural analysis, it was necessary to obtain the static X-ray scattering curve for each state. To this end, we measured the static X-ray scattering of the ground and light-activated states and constructed the species-associated scattering curves (SASs) for the intermediate states using a well-established method.[36] The details on constructing the SASs are described in Supplemental experimental procedures. As shown in Figure 3B, the difference curve from the static X-ray solution scattering data of ground and light-activated states shows good agreement with SADS3 from TRXSS data, confirming that SAXS and TRXSS experiments were performed for the same light-induced transition. The details of the structural analysis are described in Supplemental experimental procedures and Figure S10, and a brief description is given here.

In the structural analysis, the candidate structures for each state of coPYP-4 are generated by MD simulations and are used to calculate theoretical X-ray scattering curves. For each state of coPYP-4, the multiple sets of a predefined number of curves randomly selected from these theoretical curves make ensembles, and the average scattering curve of the ensemble is compared with the experimental data. The genetic algorithm (GA)[86] used in the EOM analysis allows some structures in an ensemble to propagate to the next generation, whereas others are randomly exchanged for the structures remaining in the structure pool or other ensembles. As generations are repeated, the ensembles are iteratively compared with the experimental data, and the ensemble that best describes the observed data is chosen to obtain the representative protein structure and the structural parameter of the radius of gyration (R_g).

Figure 4 shows the results of the structural analysis for each state of coPYP-4. For all states, each average scattering curve of the ensemble describes the experimental data (Figure 4). The distribution of R_g shows one major peak near 32 Å and one minor peak near 34.5 Å in the ground state (Figure 4B). Considering that the N terminus of the PYP monomer is structurally flexible even in the ground state, the distribution of R_g suggests that the flexibility of the N terminus allows coPYP-4 to form a minor

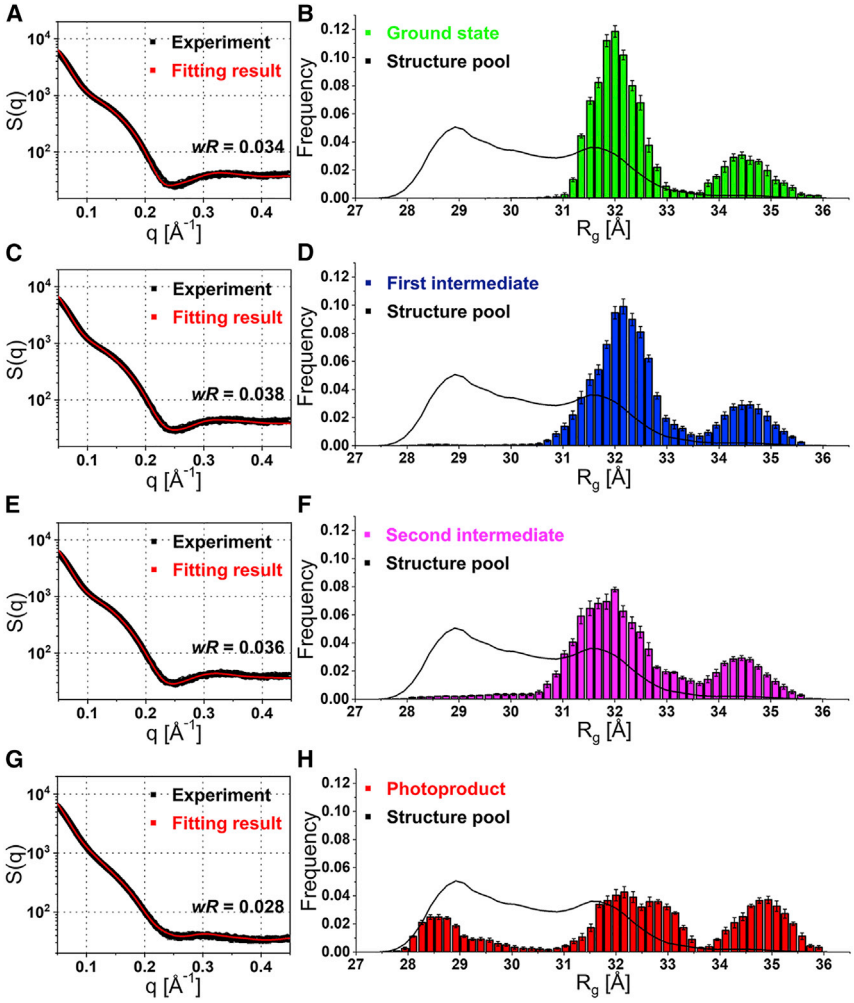

Figure 4. Results from structural analysis of static curves based on EOM

(A–H) Results of the EOM analysis for the ground state (A and B), the first intermediate (C and D), the second intermediate (E and F), and the photoproduct (G and H). The static curves of the best fitting ensemble (red) describe the experimental static curves (black) well (A, C, E, and G). For each case, the weighted R factor (wR), which quantifies the agreement between the experimental curve and the fitted curve, is shown. In the ground state, the distribution of R_g determined from the EOM analysis shows one major peak near R_g of 32 Å and one minor peak near R_g of 34 to ~35 Å (B). The major peak gradually broadens as it progresses from the ground state to the first intermediate (D), the second intermediate (F), and the photoproduct (H). In the photoproduct, a new peak near R_g of 28.5 Å appears, indicating the contraction motion of coPYP-4. Unlike the major peaks, the minor peaks were obtained similarly in all four states. In the R_g distribution of each state, the error bars are the standard deviation of the R_g distribution for the optimized ensemble calculated from repeated EOM analysis (supplemental experimental procedures).

conformation with a larger ring than the major one. As the reaction progresses, the major peak gradually broadens in the first and second intermediates (Figures 4D and 4F). In the photoproduct (the third intermediate), the major peak becomes broader than those in the first two intermediates, and a new peak appears near 28.5 Å (Figure 4H), showing that the light-induced structural transition of coPYP-4 involves a contraction motion of the protein. The representative structures for the ground state and photoproduct determined from the structural analysis represent R_g values of 31.8 and 28.6 Å, respectively (Figures 5A and 5B). Besides, comparison of the two structures shows that the distances among the PYP units are smaller in the

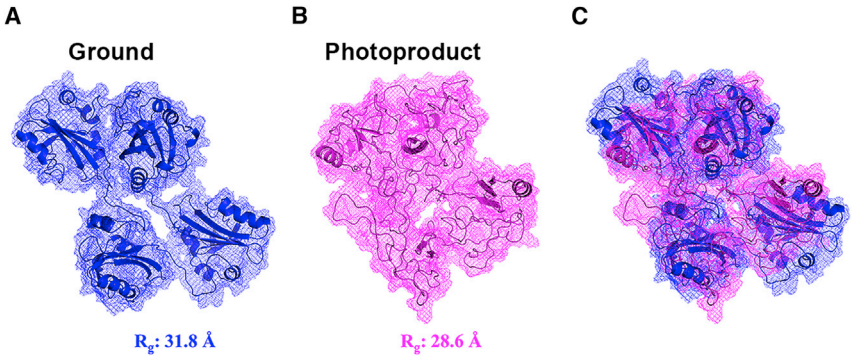

Figure 5. Representative structures for the ground state and the photoproduct of coPYP-4 from structural analysis based on EOM

(A and B) Representative structures of the ground state (A) and the photoproduct (B) have R_g values of 31.8 and 28.6 Å, respectively.

(C) Structures in (A) and (B) are overlaid for comparison. The representative structures are expressed in the cartoon and mesh styles using the PyMOL visualization tool.

photoproduct than in the ground state (Figures 5C and 5D). In the light-induced structural transition, it is also observed that some distribution of the major peak shifts from near 32 Å to near 33 Å and the minor peak shifts from near 34.5 Å to near 35 Å (Figure 4), implying that a minor population of coPYP-4 may also exhibit subtle expansion motion by light. Nevertheless, the increases of the R_g values are less than 1 Å, and the expansion motion is not as pronounced as the contraction motion. Therefore, we focus on the contraction motion for the light-induced structural changes of coPYP-4.

Effective connection among the PYP units by cPYP and the flexible GS linkers

The measured molecular weights of coPYPs show that the number of the PYP units constituting coPYPs can be controlled by our approach (Table 1). The single bands in native-PAGE and single peaks in SEC demonstrate that each coPYP does not break down into subunits or form higher oligomers, indicating that the linkers stably maintain the connections among the PYP units in coPYPs (Figure 2). In addition, the UV-visible (UV-vis) spectrum of coPYP-4 is almost identical to that of monomer PYP, implying that the linkers do not significantly affect the environment around the chromophore of the PYP units (Figure S7). These results confirm that our approach using cPYP and the flexible GS linkers effectively constructs circular oligomer proteins of various oligomer sizes without significantly affecting the environment around the chromophores of the PYP units.

Morphological shape

In SEC, the proteins pass through beads with a range of well-defined pore sizes in the course of flowing through the SEC column. Whether the proteins pass through the beads depends not only on their sizes but also on their shapes.[87] Although the molecular weights of coPYP-4 and loPYP-4 are the same, the elution profile of coPYP-4 shows a relatively smaller elution volume than that of loPYP-4, indicating that coPYP-4 has a relatively extended structure compared with that of loPYP-4 (Figure 2B). This extended structure is likely to be link to with the existence of the cavity in the center of coPYP-4, which is evident in the TEM images (Figure 2C).

Chromophore kinetics

The photocycle of monomer PYP is well established with two candidate kinetic models: the sequential and the parallel models.[33,35,36,40–44] For the TA result, we

Please cite this article in press as: Lee et al., Reversible molecular motional switch based on circular photoactive protein oligomers exhibits unexpected photo-induced contraction, Cell Reports Physical Science (2021), https://doi.org/10.1016/j.xcrp.2021.100512

focus on the kinetic similarity between monomer PYP and coPYP-4 regardless of the kinetic model. The time constants of monomer PYP determined by using TA, 6.2 μs, 280 μs, 1.3 ms, and 110 ms, can be assigned to the decay of pR_1, the $pR_2 \rightarrow pB_1$ transition, the $pB_1 \rightarrow pB_2$ transition, and the $pB_2 \rightarrow pG$ transition, respectively. Because the time constants of coPYP-4, 1.9 μs, 180 μs, 1.4 ms, and 79 ms, are similar to those of monomer PYP, the time constants of coPYP-4 can be assigned to transitions similar to those of monomer PYP. As mentioned earlier, the similarity of the UV-visible spectra of monomer PYP and coPYP-4 implies that the environments around the chromophores of the two proteins are similar in the ground state (Figure S7). Unlike the ground state, however, the TA spectra (Figure S3A) of coPYP-4 show a broader peak of negative absorption compared with those of monomer PYP, suggesting the intermediates of coPYP-4 and monomer PYP have slightly different environments near the chromophore. In addition, coPYP-4 has a slightly faster timescale for the recovery to pG (79 ms) than does monomer PYP (110 ms). However, these differences in TA results between coPYP-4 and monomer PYP are not significant. Overall, the kinetics of coPYP-4 is similar to that of monomer PYP, suggesting that the photochemical properties of monomer PYP are retained even in the PYP units constituting coPYP-4.

Structural kinetics

Based on the results obtained by our kinetic analysis on the TRXSS data, we can establish the following kinetic model for the light-induced structural changes of coPYP-4 on the microsecond to millisecond timescale,

$$G \xrightarrow{h\nu} I_1 \xrightarrow{298\ \mu s} I_2 \xrightarrow{2.55\ ms} P \xrightarrow{> 650\ ms} G,$$

where G is a ground state, I_1 and I_2 are the intermediate states, and P is the final photoproduct involved in the light-induced transition of coPYP-4. During the light-induced transition, I_1 converts into I_2 with a time constant of 298 μs, and P is formed from I_2 with a time constant of 2.55 ms. Because these time constants are similar to those of monomer PYP[36] (279 μs and 1.3 ms), it is likely that the PYP units in I_1, I_2, and P of coPYP-4 represent the structural transitions corresponding to the reaction pathway involving pR_2, pB_1, and pB_2 of monomer PYP,[36] respectively. No pronounced recovery from the photoproduct to the ground state was observed in the TRXSS data of coPYP-4 within the time window covered in this study (178 ms). We expect that the time required for structural recovery of light-induced coPYP-4 is longer than that of monomer PYP[36] (650 ms), because the overall structure of coPYP-4 is larger than that of monomer PYP. Comparing the common time constants from TA and TRXSS shows that slower kinetics were obtained in TRXSS than in TA. Considering that spectroscopy and X-ray scattering are sensitive to local structural changes around the chromophore and the global structural changes of proteins, respectively, this phenomenon demonstrates that the local structural changes around the chromophores cause changes in the global structure with a noticeable delay during the light-induced transition. Furthermore, the time constant corresponding to 1.9 μs obtained from TA is not observed in this kinetic model, showing that the decay of pR_1 for monomer PYP does not have a significant influence on the global structure of coPYP-4.

Contraction of the ring motion

Together with the spectroscopic and structural kinetics, the results from our structural analysis suggest a structural mechanism for coPYP-4. During the light-induced transition of coPYP-4, I_1 is formed from the ground state through the transition of PYP units from pG to pR_2. Subsequently, I_1 converts into I_2 using the $pR_2 \rightarrow pB_1$

transition of the PYP units.[36] For these processes, the structural dynamics of monomer PYP show that the pG → pR_2 → pB_1 transition of the PYP units includes the gradual relaxation of the N termini in the units.[33,36,38,39] Besides, the comparison of the static curves for the ground state and two intermediate states shows differences in the oscillatory features around the wide-angle region (Figure S8), which can be generally attributed to local conformational changes such as the rearrangement of the secondary structure,[60,88] indicating that the relaxation of the N termini induces the local structural changes among the PYP units in coPYP-4. Considering that broadening of the major peaks in the distributions of R_g is observed during the light-induced transition of coPYP-4 (Figure 4), we suggest that the local structural changes allow the structure of coPYP-4 to become progressively flexible as the reaction proceeds from the ground state to the two intermediates. Finally, the pB_1 → pB_2 transition of the PYP units occurs, and I_2 forms the photoproduct (P). The representative structures of the ground state and P (Figure 5) show that the structure of coPYP-4 is contracted during the light-induced transition (Figure 1C). Considering that the relaxation of the N terminus of monomer PYP is maximized in pB_2,[33,36,38] the distributions of the R_g value of P indicate that the structure of coPYP-4 contracts when its flexibility is maximized. This contraction motion involves structural changes in the opposite direction of our expectation that the light-induced N-terminal protrusion of the PYP unit would render coPYP-4 expanded. For this difference, we anticipate that the flexible structure would allow coPYP-4 to easily generate new interaction networks, such as hydrogen bond interactions or hydrophobic interactions among its residues. Such interactions would make the distances between PYP units smaller, and consequently, the structure of coPYP-4 would undergo contraction instead of expansion. A comparison of the ensemble structure of monomer PYP for the signaling state (PDB: 2KX6) and PYP units in the photoproduct of coPYP-4 shows that the N termini of PYP units of coPYP-4 exhibit relatively compact conformations compared with the N termini of monomer PYP (Figure S9). This feature is consistent with the light-induced contraction of coPYP-4.

Flexible ring protein that mimics wild-type PYP

A protein-based molecular switch is likely to retain the functional and structural characteristics of the building block proteins that compose it. From the kinetic and structural analyses of time-resolved data, we demonstrated that the light-induced perturbation of the N terminus in wild-type PYP is also observed in the monomeric units of coPYP-4, leading to the unique structural changes of coPYP-4. These observations show that coPYP-4 belongs to a mimetic protein of monomer PYP and has the feature of a new type of protein-based molecular switch. Based on the ensemble from the structural analysis (Figure 4), the broad distribution in terms of R_g can be attributed to the diversity of protein conformations because of the intrinsic flexibilities of the GS linkers and N termini.

In this study, we developed and successfully synthesized the protein-complex-based molecular switch that changes structure upon blue-light irradiation in a controllable way and experimentally verified the detailed time-dependent structural changes. The photoactivated coPYP-4 accompanies the light-induced structural changes with the contraction of a ring-shaped backbone. Using flexible linkers to connect PYP monomers made it possible to generate the contraction motion of a ring made of multiple monomers. Upon irradiation, monomer PYP undergoes only partial unfolding and protrusion of the N terminus, and the contraction motion of light-activated coPYP-4 cannot be achieved with a single PYP unit. Whereas most studies of molecular switches based on the structural information of proteins did not demonstrate real-time structural changes in a time-resolved manner, this work presents

Please cite this article in press as: Lee et al., Reversible molecular motional switch based on circular photoactive protein oligomers exhibits unexpected photo-induced contraction, Cell Reports Physical Science (2021), https://doi.org/10.1016/j.xcrp.2021.100512

how light drives the controlled structural transformation of coPYP-4 in response to blue-light irradiation at a high spatiotemporal resolution. This study may provide insights into the design and construction of protein-complex-based molecular switches with ring-shaped conformation, and the light-induced conformational changes in coPYPs may provide a new motif for the protein-based photoswitch.

EXPERIMENTAL PROCEDURES

Resource availability

Lead contact

Further information and requests for resources and reagents should be directed to and will be fulfilled by the lead contact, Hyotcherl Ihee (hyotcherl.ihee@kaist.ac.kr).

Materials availability

This study did not generate new unique reagents.

Data and code availability

All data related to this study included in the article and Supplemental information will be provided by the lead contact upon reasonable request.

Generation of coPYPs

For the generation of expression plasmids of coPYPs, the PYP linear oligomer sequences (two, three, and four PYP units) were constructed and genetically linked in the cPYP expression plasmid.[1] After generation, coPYPs were overexpressed in *Escherichia coli* BL21 (DE3) by IPTG induction, reconstituted with p-coumaric anhydride, and purified by Ni affinity chromatography and ion-exchange chromatography. The purified proteins were dialyzed with 20 mM Tris, pH 7.0, and 20 mM NaCl. The concentrations of coPYPs were determined by UV-vis spectroscopy (UV-2550; Shimadzu, Kyoto, Japan). The details of the construction and preparation of the PYP oligomers are described in Supplemental experimental procedures (Figures S1 and S2).

Time-resolved X-ray solution scattering

TRXSS data were measured at the ID14B beamline at Advanced Photon Source (Argonne, IL, USA) using a well-established method.[36,59,60] For the measurement with coPYP-4, a 1.1 mM coPYP-4 solution dissolved in 20 mM sodium phosphate buffer with 20 mM NaCl at pH 7.0 was enclosed in a quartz capillary (Hampton Research, Aliso Viejo, CA, USA). The sealed capillary was mounted on a linear translational stage (Parker, Charlotte, NC, USA) to move the capillary back and forth periodically. During the measurement, the coPYP-4 solution was irradiated by circularly polarized nanosecond laser pulses (1 mJ/mm^2 fluence at 460 nm) and was probed by X-ray pulses incident at well-defined time delays. The details of the TRXSS measurement are described in Supplemental experimental procedures.

Structural analysis

For the structural analysis using EOM, the SASs for each intermediate were constructed by adding the experimental static scattering curve of the ground state to scaled SADSs of first and second intermediates.[36] After constructing the SASs, the candidate structures for the EOM analysis were generated by running two sets of MD simulations starting from the two different initial structures obtained from the experiment-restrained rigid-body (ERRB) MD simulation.[24,45,59,66,67,89] The theoretical X-ray scattering curves were calculated from the candidate structures. Then, the theoretical X-ray scattering curves were compared with the experimental scattering curves of the ground state, first intermediate, second intermediate, and photoproduct using the EOM method to extract the structural parameter and the optimal

ensemble structures for each state.[60,81,82] The detailed procedure is described in Supplemental experimental procedures (Figure S10).

SUPPLEMENTAL INFORMATION

Supplemental information can be found online at https://doi.org/10.1016/j.xcrp.2021.100512.

ACKNOWLEDGMENTS

We thank Junbeom Jo, Sungjun Park, and Deokbeom Suh for their assistance with time-resolved x-ray scattering experiments. This work was supported by the Institute of Basic Science (IBS-R004). Transmission electron microscopy was performed at the Electron Microscopy Research Center, Korea Basic Science Institute (KBSI). The research was also supported in part by KBSI grant T38210.

AUTHOR CONTRIBUTIONS

H.I. directed the research. H.I. and Y.K. designed the research. Y.K. performed construction and basic characterization of coPYPs. Y.K., H.J., and J.H. performed the TEM experiment. Y.K. performed the static X-ray scattering experiment. S.J.L. and T.W.K. performed TRXSS experiments. C.Y. performed the TA experiment. S.J.L. and Y.K. analyzed static X-ray scattering data. S.J.L. analyzed TRXSS data. C.Y. analyzed TA data. S.J.L., C.Y., T.W.K., Y.K., and H.I. wrote the paper, and all authors discussed the experimental results.

DECLARATION OF INTERESTS

The authors declare no competing interests.

Received: May 27, 2021
Revised: June 23, 2021
Accepted: June 29, 2021
Published: July 22, 2021

REFERENCES

1. Beharry, A.A., and Woolley, G.A. (2011). Azobenzene photoswitches for biomolecules. Chem. Soc. Rev. *40*, 4422–4437.

2. Harris, J.D., Moran, M.J., and Aprahamian, I. (2018). New molecular switch architectures. Proc. Natl. Acad. Sci. USA *115*, 9414–9422.

3. Raehm, L., and Sauvage, J.-P. (2001). Molecular machines and motors based on transition metal-containing catenanes and rotaxanes. In Molecular machines and motors, J.-P. Sauvage, ed. (Springer), pp. 55–78.

4. Stein, V., and Alexandrov, K. (2015). Synthetic protein switches: design principles and applications. Trends Biotechnol. *33*, 101–110.

5. Szymański, W., Beierle, J.M., Kistemaker, H.A.V., Velema, W.A., and Feringa, B.L. (2013). Reversible photocontrol of biological systems by the incorporation of molecular photoswitches. Chem. Rev. *113*, 6114–6178.

6. Yu, J., Qi, D., and Li, J. (2020). Design, synthesis and applications of responsive macrocycles. Commun. Chem. *3*, 189.

7. Wang, Y., and Li, Q. (2012). Light-driven chiral molecular switches or motors in liquid crystals. Adv. Mater. *24*, 1926–1945.

8. Wang, H., Bisoyi, H.K., Urbas, A.M., Bunning, T.J., and Li, Q. (2019). Reversible circularly polarized reflection in a self-organized helical superstructure enabled by a visible-light-driven axially chiral molecular switch. J. Am. Chem. Soc. *141*, 8078–8082.

9. Wang, H., Bisoyi, H.K., Li, B.X., McConney, M.E., Bunning, T.J., and Li, Q. (2020). Visible-Light-Driven Halogen Bond Donor Based Molecular Switches: From Reversible Unwinding to Handedness Inversion in Self-Organized Soft Helical Superstructures. Angew. Chem. Int. Ed. Engl. *59*, 2684–2687.

10. Cannon, K.A., Nguyen, V.N., Morgan, C., and Yeates, T.O. (2020). Design and characterization of an icosahedral protein cage formed by a double-fusion protein containing three distinct symmetry elements. ACS Synth. Biol. *9*, 517–524.

11. Fletcher, J.M., Harniman, R.L., Barnes, F.R., Boyle, A.L., Collins, A., Mantell, J., Sharp, T.H., Antognozzi, M., Booth, P.J., Linden, N., et al. (2013). Self-assembling cages from coiled-coil peptide modules. Science *340*, 595–599.

12. An, Y., Wang, G., Diao, Y., Long, Y., Fu, X., Weng, M., Zhou, L., Sun, K., Cheung, T.H., Ip, N.Y., et al. (2017). A Molecular Switch Regulating Cell Fate Choice between Muscle Progenitor Cells and Brown Adipocytes. Dev. Cell *41*, 382–391.e5.

13. Gao, Z., Liu, Q., Zhang, Y., Chen, D., Zhan, X., Deng, C., Cheng, S., and Cao, L. (2020). OsCUL3a-Associated Molecular Switches Have Functions in Cell Metabolism, Cell Death, and Disease Resistance. J. Agric. Food Chem. *68*, 5471–5482.

14. Noyes, N.C., Walkinshaw, E., and Davis, R.L. (2020). Ras acts as a molecular switch between two forms of consolidated memory in *Drosophila*. Proc. Natl. Acad. Sci. USA *117*, 2133–2139.

15. Tafoya, S., and Bustamante, C. (2018). Molecular switch-like regulation in motor proteins. Philos. Trans. R. Soc. Lond. B Biol. Sci. *373*, 20170181.

16. Taylor, J.L., Rohatgi, P., Spencer, H.T., Doyle, D.F., and Azizi, B. (2010). Characterization of a

molecular switch system that regulates gene expression in mammalian cells through a small molecule. BMC Biotechnol. *10*, 15.

17. Vogel, M., Bukau, B., and Mayer, M.P. (2006). Allosteric regulation of Hsp70 chaperones by a proline switch. Mol. Cell *21*, 359–367.

18. Hörner, M., and Weber, W. (2012). Molecular switches in animal cells. FEBS Lett. *586*, 2084–2096.

19. Etzl, S., Lindner, R., Nelson, M.D., and Winkler, A. (2018). Structure-guided design and functional characterization of an artificial red light-regulated guanylate/adenylate cyclase for optogenetic applications. J. Biol. Chem. *293*, 9078–9089.

20. Kim, Y., Ganesan, P., and Ihee, H. (2013). High-throughput instant quantification of protein expression and purity based on photoactive yellow protein turn off/on label. Protein Sci. *22*, 1109–1117.

21. Kumar, A., Burns, D.C., Al-Abdul-Wahid, M.S., and Woolley, G.A. (2013). A circularly permuted photoactive yellow protein as a scaffold for photoswitch design. Biochemistry *52*, 3320–3331.

22. Miyawaki, A., Llopis, J., Heim, R., McCaffery, J.M., Adams, J.A., Ikura, M., and Tsien, R.Y. (1997). Fluorescent indicators for Ca2+ based on green fluorescent proteins and calmodulin. Nature *388*, 882–887.

23. Pudasaini, A., El-Arab, K.K., and Zoltowski, B.D. (2015). LOV-based optogenetic devices: light-driven modules to impart photoregulated control of cellular signaling. Front. Mol. Biosci. *2*, 18.

24. Kim, Y., Yang, C., Kim, T.W., Thamilselvan, K., Kim, Y., and Ihee, H. (2018). Regulation of Protein Structural Changes by Incorporation of a Small-Molecule Linker. Int. J. Mol. Sci. *19*, 3714.

25. Campos, L.A., Sharma, R., Alvira, S., Ruiz, F.M., Ibarra-Molero, B., Sadqi, M., Alfonso, C., Rivas, G., Sanchez-Ruiz, J.M., Romero Garrido, A., et al. (2019). Engineering protein assemblies with allosteric control via monomer fold-switching. Nat. Commun. *10*, 5703.

26. Kawano, F., Suzuki, H., Furuya, A., and Sato, M. (2015). Engineered pairs of distinct photoswitches for optogenetic control of cellular proteins. Nat. Commun. *6*, 6256.

27. Morgan, S.-A., Al-Abdul-Wahid, S., and Woolley, G.A. (2010). Structure-based design of a photocontrolled DNA binding protein. J. Mol. Biol. *399*, 94–112.

28. Weber, W., and Fussenegger, M. (2011). Molecular diversity—the toolbox for synthetic gene switches and networks. Curr. Opin. Chem. Biol. *15*, 414–420.

29. Chen, Y.Y., Jensen, M.C., and Smolke, C.D. (2010). Genetic control of mammalian T-cell proliferation with synthetic RNA regulatory systems. Proc. Natl. Acad. Sci. USA *107*, 8531–8536.

30. Xie, Z., Wroblewska, L., Prochazka, L., Weiss, R., and Benenson, Y. (2011). Multi-input RNAi-based logic circuit for identification of specific cancer cells. Science *333*, 1307–1311.

31. Trabi, M., and Craik, D.J. (2002). Circular proteins—no end in sight. Trends Biochem. Sci. *27*, 132–138.

32. Borgstahl, G.E., Williams, D.R., and Getzoff, E.D. (1995). 1.4 A structure of photoactive yellow protein, a cytosolic photoreceptor: unusual fold, active site, and chromophore. Biochemistry *34*, 6278–6287.

33. Cho, H.S., Schotte, F., Dashdorj, N., Kyndt, J., Henning, R., and Anfinrud, P.A. (2016). Picosecond photobiology: watching a signaling protein function in real time via time-resolved small- and wide-angle X-ray scattering. J. Am. Chem. Soc. *138*, 8815–8823.

34. Genick, U.K., Borgstahl, G.E., Ng, K., Ren, Z., Pradervand, C., Burke, P.M., Šrajer, V., Teng, T.Y., Schildkamp, W., McRee, D.E., et al. (1997). Structure of a protein photocycle intermediate by millisecond time-resolved crystallography. Science *275*, 1471–1475.

35. Ihee, H., Rajagopal, S., Šrajer, V., Pahl, R., Anderson, S., Schmidt, M., Schotte, F., Anfinrud, P.A., Wulff, M., and Moffat, K. (2005). Visualizing reaction pathways in photoactive yellow protein from nanoseconds to seconds. Proc. Natl. Acad. Sci. USA *102*, 7145–7150.

36. Kim, T.W., Lee, J.H., Choi, J., Kim, K.H., van Wilderen, L.J., Guerin, L., Kim, Y., Jung, Y.O., Yang, C., Kim, J., et al. (2012). Protein structural dynamics of photoactive yellow protein in solution revealed by pump-probe X-ray solution scattering. J. Am. Chem. Soc. *134*, 3145–3153.

37. Larsen, D.S., Vengris, M., van Stokkum, I.H., van der Horst, M.A., de Weerd, F.L., Hellingwerf, K.J., and van Grondelle, R. (2004). Photoisomerization and photoionization of the photoactive yellow protein chromophore in solution. Biophys. J. *86*, 2538–2550.

38. Ramachandran, P.L., Lovett, J.E., Carl, P.J., Cammarata, M., Lee, J.H., Jung, Y.O., Ihee, H., Timmel, C.R., and van Thor, J.J. (2011). The short-lived signaling state of the photoactive yellow protein photoreceptor revealed by combined structural probes. J. Am. Chem. Soc. *133*, 9395–9404.

39. van der Horst, M.A., van Stokkum, I.H., Crielaard, W., and Hellingwerf, K.J. (2001). The role of the N-terminal domain of photoactive yellow protein in the transient partial unfolding during signalling state formation. FEBS Lett. *497*, 26–30.

40. Hoshihara, Y., Imamoto, Y., Kataoka, M., Tokunaga, F., and Terazima, M. (2008). Conformational changes in the N-terminal region of photoactive yellow protein: a time-resolved diffusion study. Biophys. J. *94*, 2187–2193.

41. Imamoto, Y., Kamikubo, H., Harigai, M., Shimizu, N., and Kataoka, M. (2002). Light-induced global conformational change of photoactive yellow protein in solution. Biochemistry *41*, 13595–13601.

42. Khan, J.S., Imamoto, Y., Harigai, M., Kataoka, M., and Terazima, M. (2006). Conformational changes of PYP monitored by diffusion coefficient: effect of N-terminal α-helices. Biophys. J. *90*, 3686–3693.

43. Schotte, F., Cho, H.S., Kaila, V.R., Kamikubo, H., Dashdorj, N., Henry, E.R., Graber, T.J., Henning, R., Wulff, M., Hummer, G., et al. (2012). Watching a signaling protein function in real time via 100-ps time-resolved Laue crystallography. Proc. Natl. Acad. Sci. USA *109*, 19256–19261.

44. Yeremenko, S., van Stokkum, I.H., Moffat, K., and Hellingwerf, K.J. (2006). Influence of the crystalline state on photoinduced dynamics of photoactive yellow protein studied by ultraviolet-visible transient absorption spectroscopy. Biophys. J. *90*, 4224–4235.

45. Kim, Y., Ganesan, P., Jo, J., Kim, S.O., Thamilselvan, K., and Ihee, H. (2018). Chromophore-removal-induced conformational change in photoactive yellow protein determined through spectroscopic and X-ray solution scattering studies. J. Phys. Chem. B *122*, 4513–4520.

46. Mizuno, M., Hamada, N., Tokunaga, F., and Mizutani, Y. (2007). Picosecond protein response to the chromophore isomerization of photoactive yellow protein: selective observation of tyrosine and tryptophan residues by time-resolved ultraviolet resonance Raman spectroscopy. J. Phys. Chem. B *111*, 6293–6296.

47. Mizuno, M., Kamikubo, H., Kataoka, M., and Mizutani, Y. (2011). Changes in the hydrogen-bond network around the chromophore of photoactive yellow protein in the ground and excited states. J. Phys. Chem. B *115*, 9306–9310.

48. Meyer, T.E., Yakali, E., Cusanovich, M.A., and Tollin, G. (1987). Properties of a water-soluble, yellow protein isolated from a halophilic phototrophic bacterium that has photochemical activity analogous to sensory rhodopsin. Biochemistry *26*, 418–423.

49. Wang, D., Li, X., Wang, L., Yang, X., and Zhong, D. (2020). Elucidating Ultrafast Multiphasic Dynamics in the Photoisomerization of Cyanobacteriochrome. J. Phys. Chem. Lett. *11*, 8819–8824.

50. Wang, D., Qin, Y., Zhang, M., Li, X., Wang, L., Yang, X., and Zhong, D. (2020). The Origin of Ultrafast Multiphasic Dynamics in Photoisomerization of Bacteriophytochrome. J. Phys. Chem. Lett. *11*, 5913–5919.

51. Akiyama, S., Takahashi, S., Kimura, T., Ishimori, K., Morishima, I., Nishikawa, Y., and Fujisawa, T. (2002). Conformational landscape of cytochrome c folding studied by microsecond-resolved small-angle x-ray scattering. Proc. Natl. Acad. Sci. USA *99*, 1329–1334.

52. Konuma, T., Kimura, T., Matsumoto, S., Goto, Y., Fujisawa, T., Fersht, A.R., and Takahashi, S. (2011). Time-resolved small-angle X-ray scattering study of the folding dynamics of barnase. J. Mol. Biol. *405*, 1284–1294.

53. Stagno, J.R., Liu, Y., Bhandari, Y.R., Conrad, C.E., Panja, S., Swain, M., Fan, L., Nelson, G., Li, C., Wendel, D.R., et al. (2017). Structures of riboswitch RNA reaction states by mix-and-inject XFEL serial crystallography. Nature *541*, 242–246.

54. Zuo, X., Wang, J., Yu, P., Eyler, D., Xu, H., Starich, M.R., Tiede, D.M., Simon, A.E., Kasprzak, W., Schwieters, C.D., et al. (2010). Solution structure of the cap-independent translational enhancer and ribosome-binding

element in the 3′ UTR of turnip crinkle virus. Proc. Natl. Acad. Sci. USA *107*, 1385–1390.

55. Andersson, M., Malmerberg, E., Westenhoff, S., Katona, G., Cammarata, M., Wöhri, A.B., Johansson, L.C., Ewald, F., Eklund, M., Wulff, M., et al. (2009). Structural dynamics of light-driven proton pumps. Structure *17*, 1265–1275.

56. Björling, A., Berntsson, O., Lehtivuori, H., Takala, H., Hughes, A.J., Panman, M., Hoernke, M., Niebling, S., Henry, L., Henning, R., et al. (2016). Structural photoactivation of a full-length bacterial phytochrome. Sci. Adv. *2*, e1600920.

57. Cammarata, M., Levantino, M., Schotte, F., Anfinrud, P.A., Ewald, F., Choi, J., Cupane, A., Wulff, M., and Ihee, H. (2008). Tracking the structural dynamics of proteins in solution using time-resolved wide-angle X-ray scattering. Nat. Methods *5*, 881–886.

58. Heyes, D.J., Hardman, S.J.O., Pedersen, M.N., Woodhouse, J., De La Mora, E., Wulff, M., Weik, M., Cammarata, M., Scrutton, N.S., and Schirò, G. (2019). Light-induced structural changes in a full-length cyanobacterial phytochrome probed by time-resolved X-ray scattering. Commun. Biol. *2*, 1–8.

59. Kim, K.H., Muniyappan, S., Oang, K.Y., Kim, J.G., Nozawa, S., Sato, T., Koshihara, S.Y., Henning, R., Kosheleva, I., Ki, H., et al. (2012). Direct observation of cooperative protein structural dynamics of homodimeric hemoglobin from 100 ps to 10 ms with pump-probe X-ray solution scattering. J. Am. Chem. Soc. *134*, 7001–7008.

60. Kim, T.W., Lee, S.J., Jo, J., Kim, J.G., Ki, H., Kim, C.W., Cho, K.H., Choi, J., Lee, J.H., Wulff, M., et al. (2020). Protein folding from heterogeneous unfolded state revealed by time-resolved X-ray solution scattering. Proc. Natl. Acad. Sci. USA *117*, 14996–15005.

61. Panman, M.R., Biasin, E., Berntsson, O., Hermann, M., Niebling, S., Hughes, A.J., Kübel, J., Atkovska, K., Gustavsson, E., Nimmrich, A., et al. (2020). Observing the structural evolution in the photodissociation of diiodomethane with femtosecond solution x-ray scattering. Phys. Rev. Lett. *125*, 226001.

62. Rimmerman, D., Leshchev, D., Hsu, D.J., Hong, J., Kosheleva, I., and Chen, L.X. (2017). Direct observation of insulin association dynamics with time-resolved X-ray scattering. J. Phys. Chem. Lett. *8*, 4413–4418.

63. Takala, H., Björling, A., Berntsson, O., Lehtivuori, H., Niebling, S., Hoernke, M., Kosheleva, I., Henning, R., Menzel, A., Ihalainen, J.A., and Westenhoff, S. (2014). Signal amplification and transduction in phytochrome photosensors. Nature *509*, 245–248.

64. Arnlund, D., Johansson, L.C., Wickstrand, C., Barty, A., Williams, G.J., Malmerberg, E., Davidsson, J., Milathianaki, D., DePonte, D.P., Shoeman, R.L., et al. (2014). Visualizing a protein quake with time-resolved X-ray scattering at a free-electron laser. Nat. Methods *11*, 923–926.

65. Ravishankar, H., Pedersen, M.N., Eklund, M., Sitsel, A., Li, C., Duelli, A., Levantino, M., Wulff, M., Barth, A., Olesen, C., et al. (2020). Tracking Ca^{2+} ATPase intermediates in real time by x-ray solution scattering. Sci. Adv. *6*, eaaz0981.

66. Lee, Y., Kim, J.G., Lee, S.J., Muniyappan, S., Kim, T.W., Ki, H., Kim, H., Jo, J., Yun, S.R., Lee, H., et al. (2021). Ultrafast coherent motion and helix rearrangement of homodimeric hemoglobin visualized with femtosecond X-ray solution scattering. Nat. Commun. *12*, 3677.

67. Kim, J.G., Kim, T.W., Kim, J., and Ihee, H. (2015). Protein structural dynamics revealed by time-resolved X-ray solution scattering. Acc. Chem. Res. *48*, 2200–2208.

68. Kim, K.H., Kim, J.G., Nozawa, S., Sato, T., Oang, K.Y., Kim, T.W., Ki, H., Jo, J., Park, S., Song, C., et al. (2015). Direct observation of bond formation in solution with femtosecond X-ray scattering. Nature *518*, 385–389.

69. Kim, J.G., Nozawa, S., Kim, H., Choi, E.H., Sato, T., Kim, T.W., Kim, K.H., Ki, H., Kim, J., Choi, M., et al. (2020). Mapping the emergence of molecular vibrations mediating bond formation. Nature *582*, 520–524.

70. Biasin, E., van Driel, T.B., Kjær, K.S., Dohn, A.O., Christensen, M., Harlang, T., Chabera, P., Liu, Y., Uhlig, J., Pápai, M., et al. (2016). Femtosecond X-Ray Scattering Study of Ultrafast Photoinduced Structural Dynamics in Solvated [Co(terpy)_2]^2+. Phys. Rev. Lett. *117*, 013002.

71. van Driel, T.B., Kjær, K.S., Hartsock, R.W., Dohn, A.O., Harlang, T., Chollet, M., Christensen, M., Gawelda, W., Henriksen, N.E., Kim, J.G., et al. (2016). Atomistic characterization of the active-site solvation dynamics of a model photocatalyst. Nat. Commun. *7*, 13678.

72. Ihee, H. (2009). Visualizing solution-phase reaction dynamics with time-resolved X-ray liquidography. Acc. Chem. Res. *42*, 356–366.

73. Ihee, H., Lorenc, M., Kim, T.K., Kong, Q.Y., Cammarata, M., Lee, J.H., Bratos, S., and Wulff, M. (2005). Ultrafast x-ray diffraction of transient molecular structures in solution. Science *309*, 1223–1227.

74. Hsu, D.J., Leshchev, D., Rimmerman, D., Hong, J., Kelley, M.S., Kosheleva, I., Zhang, X., and Chen, L.X. (2019). X-ray snapshots reveal conformational influence on active site ligation during metalloprotein folding. Chem. Sci. (Camb.) *10*, 9788–9800.

75. Neutze, R., and Moffat, K. (2012). Time-resolved structural studies at synchrotrons and X-ray free electron lasers: opportunities and challenges. Curr. Opin. Struct. Biol. *22*, 651–659.

76. Neutze, R., Wouts, R., Techert, S., Davidsson, J., Kocsis, M., Kirrander, A., Schotte, F., and Wulff, M. (2001). Visualizing photochemical dynamics in solution through picosecond x-ray scattering. Phys. Rev. Lett. *87*, 195508.

77. Kunnus, K., Vacher, M., Harlang, T.C.B., Kjær, K.S., Haldrup, K., Biasin, E., van Driel, T.B., Pápai, M., Chabera, P., Liu, Y., et al. (2020). Vibrational wavepacket dynamics in Fe carbene photosensitizer determined with femtosecond X-ray emission and scattering. Nat. Commun. *11*, 634.

78. Haldrup, K., Levi, G., Biasin, E., Vester, P., Laursen, M.G., Beyer, F., Kjær, K.S., Brandt van Driel, T., Harlang, T., Dohn, A.O., et al. (2019). Ultrafast X-Ray Scattering Measurements of Coherent Structural Dynamics on the Ground-State Potential Energy Surface of a Diplatinum Molecule. Phys. Rev. Lett. *122*, 063001.

79. Kjær, K.S., Van Driel, T.B., Harlang, T.C.B., Kunnus, K., Biasin, E., Ledbetter, K., Hartsock, R.W., Reinhard, M.E., Koroidov, S., Li, L., et al. (2019). Finding intersections between electronic excited state potential energy surfaces with simultaneous ultrafast X-ray scattering and spectroscopy. Chem. Sci. (Camb.) *10*, 5749–5760.

80. Christensen, M., Haldrup, K., Bechgaard, K., Feidenhans'l, R., Kong, Q., Cammarata, M., Lo Russo, M., Wulff, M., Harrit, N., and Nielsen, M.M. (2009). Time-resolved X-ray scattering of an electronically excited state in solution. Structure of the 3A(2u) state of tetrakis-mu-pyrophosphitodiplatinate(II). J. Am. Chem. Soc. *131*, 502–508.

81. Bernadó, P., Mylonas, E., Petoukhov, M.V., Blackledge, M., and Svergun, D.I. (2007). Structural characterization of flexible proteins using small-angle X-ray scattering. J. Am. Chem. Soc. *129*, 5656–5664.

82. Bernadó, P., and Svergun, D.I. (2012). Structural analysis of intrinsically disordered proteins by small-angle X-ray scattering. Mol. Biosyst. *8*, 151–167.

83. Yang, C., Choi, M., Kim, J.G., Kim, H., Muniyappan, S., Nozawa, S., Adachi, S.I., Henning, R., Kosheleva, I., and Ihee, H. (2018). Protein Structural Dynamics of Wild-Type and Mutant Homodimeric Hemoglobin Studied by Time-Resolved X-Ray Solution Scattering. Int. J. Mol. Sci. *19*, 3633.

84. Yang, C., Kim, S.O., Kim, Y., Yun, S.R., Choi, J., and Ihee, H. (2017). Photocycle of photoactive yellow protein in cell-mimetic environments: molecular volume changes and kinetics. J. Phys. Chem. B *121*, 769–779.

85. Düx, P., Rubinstenn, G., Vuister, G.W., Boelens, R., Mulder, F.A., Hård, K., Hoff, W.D., Kroon, A.R., Crielaard, W., Hellingwerf, K.J., and Kaptein, R. (1998). Solution structure and backbone dynamics of the photoactive yellow protein. Biochemistry *37*, 12689–12699.

86. Jones, G. (1998). Genetic and evolutionary algorithms. In Encyclopedia of Computational Chemistry, *Volume 2*, P. von Ragué Schleyer, ed. Encyclopedia of Computational Chemistry (Wiley), pp. 1127–1136.

87. Irvine, G.B. (2000). Determination of molecular size by size-exclusion chromatography (gel filtration). Curr. Protoc. Cell Biol. *6*, 5.5.1–5.5.16.

88. Kim, T.W., Yang, C., Kim, Y., Kim, J.G., Kim, J., Jung, Y.O., Jun, S., Lee, S.J., Park, S., Kosheleva, I., et al. (2016). Combined probes of X-ray scattering and optical spectroscopy reveal how global conformational change is temporally and spatially linked to local structural perturbation in photoactive yellow protein. Phys. Chem. Chem. Phys. *18*, 8911–8919.

89. Ahn, S., Kim, K.H., Kim, Y., Kim, J., and Ihee, H. (2009). Protein tertiary structural changes visualized by time-resolved X-ray solution scattering. J. Phys. Chem. B *113*, 13131–13133.